Green Treatment and Artificial Neural Networks for the breakthrough analysis of single and multi-variant elements

Padmaja M.* and Bhavani R.
Department of Civil Engineering, Jawaharlal Nehru Technological University, Anantapuramu, INDIA
*padmajamegham@gmail.com

Abstract

Activated carbon prepared from potassium hydroxide (KOH) modified vetiver roots (VAC) was tested for its effectiveness in the single and multi-variant element sorption of three metal ions Pb^{+2}, Cd^{+2} and Ni^{+2}. The chemical and morphological characteristics of VAC were examined using Fourier Transform Infrared spectroscopy (FTIR) and Scanning electron microscopy (SEM). Continuous fixed-bed column studies were performed on single and binary metal solutions at pH 6.5, bed depth 10 cm, flow rate 5 mL min^{-1} for 10 hours. The experimental breakthrough parameters revealed maximum q_{bed} of 0.59 mg g^{-1} for Ni^{+2} in single and 0.55 mg g^{-1} for Cd^{+2} in binary (Pb^{+2}-Cd^{+2}) solutions respectively.

Four artificial neural networks (ANNs) FFBP, FFBP-DTD, Cascade and Elman models were used for fitting and simulating the breakthrough adsorption. Results showed that FFBP and Cascade ANNs models validated well with the test results and were reliable in representing the highly uneven performance of concentration outlines in both single and binary metal-ion solutions breakthrough curves.

Keywords: Vetiver, metal-ions, adsorption, fixed-bed, breakthrough, ANNs.

Introduction

Industries employing heavy metals often generate effluents which pose a danger to human health and also to aquatic life when discharged into natural water bodies[13]. Lead (Pb) enters the water environment from numerous industries resulting in diseases like anaemia, brain injury, anorexia and loss of appetite [6]. A study reported that acute and chronic disorders like kidney failure, nervous system break down, failure of the liver and cardiovascular system are caused by high-level exposure to Cadmium (Cd)[26].

Higher concentrations Nickel (Ni) results in several health issues like dermatitis, chest pain, lung cancer, renal disorders, gastrointestinal illness, palpitations, and intense weakness[21]. The effectiveness of multi-metal adsorption in aqueous solutions has been substantiated under the influence of competitive-ions and is antagonistic and accounts for reduction in the acceptance of other ions[11,14]. The number and concentration of each of the metal-ions decide the antagonistic (i.e. competitive) adsorption process[14]. In packed-bed columns, it is highly challenging to model the antagonistic behaviour of multi-metal ions as a result of non-linear adsorption effect resulting in high degree of asymmetrical breakthrough curves[25]. Conventional modelling and optimization techniques were mostly time-consuming and tiresome, also lead to misinterpretation of the multi-component breakthrough curve results, and were unsuccessful[19].

In recent times, there has been extensive interest on artificial neural networks (ANNs) employed in modelling, optimization and simulation of adsorption processes and their performance at variable operating circumstances[8, 15]. ANNs are most prominent and reliable in depicting the non-linear relations between variables[23]. Recently, most of the adsorption studies employed ANNs for data fitting and modelling of breakthrough curves[4, 5].

ANNs were compared against experimentally obtained batch kinetics of multi-component removal computational efficiency[9]. MLP network in ANNs was used for studying sorption kinetics in the multi-component system of Cu^{+2}, Zn^{+2} and Cr^{+6}.[22] Although ANNs are beneficial, its drawbacks of bone char on multi-variant element sorption in binary, ternary and quaternary mixtures were investigated[17]. There have been a large array of improvements achieved in last few years using ANNs, one of which is the dynamic fuzzy neural network for multi-component adsorption.[10]

ANNs model results demonstrate potential superiority in showing the maximum modelling errors than the experimental breakthrough analysis for multi-component removal of Cu^{2+} and Zn^{2+} ions[12]. The current study highlights the preparation and utilization of vetiver activated carbon (VAC) for the removal of multi-variant ions from wastewater.

This investigation targets modelling and optimization of the experimental multi-metal adsorption breakthrough curves on *vetiver* activated carbon in fixed-bed columns and their comparison with ANNs.

This work also evaluates four ANNs surrogate models (Feed forward back propagation, Feed forward back propagation with a distributed time delay, Cascade neural network and Elman neural network) applied to experimental data. The fixed bed column adsorption breakthrough modelling for Lead (Pb^{+2}), Cadmium (Cd^{+2}), and Nickel (Ni^{+2}) ions in single and binary solutions was performed.

Material and Methods

Adsorbates and adsorbents for a fixed-bed column: Stock solutions (1000 ppm) from pure grade nitrate salts of Lead, Cadmium and Nickel were prepared. *Vetiveria zizanioides* roots were obtained from a local market in Andhra Pradesh. *Vetiver* roots were cleaned thoroughly and 100 grams of dried and roughly crushed roots were soaked in 1:1 w/w KOH for 24 hours. Subsequently, the material was shifted to a crucible, followed by heating at 550 ºC under N_2 atmosphere for complete carbonization. After cooling, the obtained material was called the *vetiver* activated carbon (VAC), it was pulverized, sieved (<200 μm) and accumulated in airtight bags for subsequent studies.

An FTIR spectrum of VAC, at different temperatures, is shown in fig. 1. The spectrum of the *vetiver* roots exhibited functional groups of bands between 3491-3444 cm^{-1}which is assigned to amides or carboxylic acids. The wavenumber 1629.90 cm^{-1} showed that it had been assigned to be aldehydes or carboxylic acids, functional group. The peaks at wavenumber 2956.97 cm^{-1} show that it has alkanes and alkyl functional group. It thus envisages that these functional groups existing on VAC surface engage in adsorption of the target metal.

The analysis of surface morphology was obtained using SEM micrographs of VZR-AC show considerable porosity on the surface of the sample. A significant number of macro, meso and micro pores was distributed over the entire surface of the micrograph. A notable pore width was witnessed in the micrographs (x2.5K and x50K) of these surface regions as shown in fig. 2.

Fixed-bed column sorption: Single-component and multi-component experimental studies were conducted in micro-columns of diameter 1.2 cm, and the depth of VAC bed was kept 10 cm. Fixed-bed columns were used in this study with a VAC packing of 9 gms having a porosity of 25 % by the up-flow mode by the aid of a peristaltic pump at chosen pH (6.5) and flow rate (5 mL min^{-1}) throughout the experiments. The feed concentration of metal was 20 mg L^{-1} which was quantified by atomic absorption spectrometry for influent as well as for effluent concentrations.

De-ionized water was run through the VAC bed 2 hrs before the experimentation to expel air from the bed. Experiments were conducted for single and binary metal solutions and duplicated to reduce the error and the mean values were plotted for the experimental breakthrough curves for an operating time up to 10 hours. Four experimental breakthrough curves were plotted, one for single metal-ion, 3 for each of the binary mixtures. Different parameters of breakthrough curves were studied, which included the breakthrough time (t_b), the saturation time (t_s), the bed adsorption capacity (q_{bed}) and the retardation factors (r_f) for both single and binary solutions.

$$t\Big|_{(Metal)_{t_{oper}}} = [0.2(Metal)_o]$$

$$t_s = t\Big|_{(Metal)_{t_{oper}}} = 0.8(Metal)_o t_b$$

$$q_{bed} = \int_{t=0}^{t=t_{oper}} \left[\frac{(Metal)_o - (Metal)_t}{m_{bed}} \right] Qdt$$

$$r_f = \frac{v_{50\%}}{AL \in}$$

Data used in ANNs: ANNs used 180 experimental data analyzed in three sections: the training set, validation set and test set of 70%, 15% and 15% respectively. Generally, ANNs models comprise of a predefined and organized network structure having a set of input, hidden and output laye[7].

The breakthrough analysis of multi-metal adsorption on VAxC was trained, tested and simulated using four ANNs surrogate models i.e. FFBP, FFBP-DTD, Cascade and Elman. A brief interpretation of these four ANNs models according to the Mat lab® environment was illustrated in fig. 3.

Feed-forward back propagation Network: Feedforward back propagation neural network FFBP shown in fig. 3a is the standard model employed in the analysis of data and its performance in terms of correlation and prediction.[20,21] The system is categorized network setup which comprises of input, hidden and output layers with variable neurons in each layer. This FFBP model is described in equation given below:

$$X_b^{c+1} = f\left(\sum_{a=1}^{N} Y_a^c w_{ab}^c + b_a^c \right)$$

where X_b^{c+1} is the output vector, Y_a^c is the input vector of the network, w_{ab}^c is the weight of the vector, b_a^c is the bias vector of the network model for a =1,.....N, c is hidden and the output layer number, it should be noted that N is the number of inputs to the neuron in the network and f is the activation function.

Feedforward back propagation neural network with a distributed time delay (FFBP-DTD): FFBP-DTD is an improvement over the FFBP model shown in fig. 3b where in each layer of the network, time is fixed by holding the input in time-delay lines which allow the model to possess a limited dynamic response[2,7]. Different values of delays were permitted in each of the network's layers. FFBP-DTD model is described in the subsequent equations:

$$H^r(t) = f\left(\sum_{b=1}^{B}\left[\sum_{d=0}^{N1} Y^b(t-d)v_{bd}^r + j_b^r\right]\right) = 1,\ldots \mathrm{R}$$

$$Y^r(t) = f\left(\sum_{a=1}^{A}\left[\sum_{d=0}^{N2} H^a(t-d)w_{ad}^b + b_a^b\right]\right) b = 1,\ldots B$$

where Y^b and H^a are the input and the output vectors in the hidden layer; H^r and Y^r are the output vectors in the output layer, v_{bd}^r and w_{ad}^b are the weights of the output and hidden layers, j_b^r and b_a^b are the related bias vectors, N_1 N_2 are the number of delays preset to 2 for each and every subsequent computations.

Cascade forward neural network (Cascade): Cascade Forward neural network shown in fig. 3c has similarity to feed forward networks, although it includes connections from the input to each previous layer to the successive layers. If a network has three layers, the input layer is well linked straight to the output layer along with the hidden layer[1,16]. This model-based equation are given below.

$$Y_b = f\left(\sum_{a=1}^{N} X_a w_a + b_1\right)$$

$$H_c = f\left(\sum_{b=1}^{M} Y_b w_b + \sum_{a=1}^{N} X_a w_a + b_2\right)$$

where X_a is the input vector in the network, w_a being the weights, b_1 and b_2 being the bias functions, Y_b and H_c are the output neurons from the hidden and the output layer; lastly *N* and *M* are the corresponding number of neurons.

Elman neural network (Elman): The Elman ANNs model, shown in fig. 3d is a concept based memory model which has specific units known as context units which help in storing the previous outputs in the hidden layer by an assured response mechanism. Every unit of the hidden layer contains an additional context unit which remains entirely linked to every hidden neuron[20,24]. Elman model-based equations are given below:

$$X_b(t) = f\left(\sum_{r=1}^{h}\sum_{b=1}^{h} Y_{br} X_r(t-1) + \sum_{a=1}^{n}\sum_{b=1}^{h} Z_{ba} S_a(t)\right)$$

$$V_c(t) = g\left(\sum_{b=1}^{h}\sum_{c=1}^{v} W_{cb} X_b(t)\right)$$

where $X_b(t)$ is the output of the hidden neuron, $b \in [1,h]$ $S_a(t)$ is the input data fed to the neuron $a \in [1,n]$, $V_c(t)$ happens to be the output data fed to the neuron $c \in [1,v]$ at time t. Z_{ba}, Y_{br} and W_{cb} are the weights assigned to the hidden neurons. Lastly, f and g are the activation functions.

Results and Discussion

Characterization of adsorbent: Fig.1 shows the FTIR spectra of the *vetiver* roots activated carbon at different temperatures. The VAC spectrum displayed bands at 3516 cm^{-1} which may be recognized as the OH stretching vibrations. Fig. 1 also presents the highest point at 334 cm^{-1} consistent to N-H, peak at 2926 cm^{-1} denotes CH_3, CH_2 and CH, highest point at 1636 cm^{-1} and 1562 cm^{-1} shows C=C with NH_2 bending vibrations, peak at 1404 cm^{-1} indicates CH_2 and CH_3 deformation, O-H and CH_2 bending vibrations. Alcohols & phenols, amines, alkanes, arenes, aldehydes and ketones are the resulting functional groups on VAC. Hence, the functional groups are expected to help in the adsorption of target metal ions.

The porous morphological structure of VAC was studied using SEM (Hitachi S-3700 model, Voltage 30 kV, Magnification x55 and a working distance of 8000 µm). Fig. 2 shows SEM images of VAC observed at two magnifications 200 µm and 10 µm showing visible surface pores which can probably adsorb the target metal-ions in this study.

Breakthrough Curves adsorption Modeling with ANNs: The packed-bed studies experiments were performed at a pH 6.5, a flow rate of 5 ml min^{-1}, a bed depth confining to 10 cm, the initial concentration of the metal-ions in the single and binary solutions being 20 ppm. Experimental breakthrough curves in the breakthrough time interval of 30 mins, the *Ct/Co* values are given in fig. 4. The breakthrough analysis was performed on bed adsorption capacities and retardation factors was reported in table 1.

At operating conditions, the metal-ion bed adsorption capacities for single and binary feeds ranged from 0.38 to 0.59, 0.24 to 0.55 mg g^{-1} respectively. The experiments revealed that the adsorption onto VAC was higher for metals in single solutions than for binary solutions in column feed.

In single-column feeds, Ni^{2+}(0.59 mg g^{-1}) and in binary feed (Pb^{2+}-Cd^{2+}) Cd^{2+}(0.55 mg g^{-1}) obtained highest adsorption capacities. Values obtained for r_f were 530.59, 631.41, 769.36 in single and 716.31–848.96 in binary column feeds. Retardation factors for binary metal feeds were lower to single metal feeds.

The breakthrough time was studied at C_t = 0.2C0 and are shown in tables 1 and 2 for single and binary column feeds, which ranged from 2 to 4 hrs and resulted as single> binary feeds. Saturation time t_s (i.e. $C_t \geq 0.8C_0$) was maximum at 8.86 hrs for Ni^{+2} in a single feed and showed a decreasing trend for the binary mixtures.

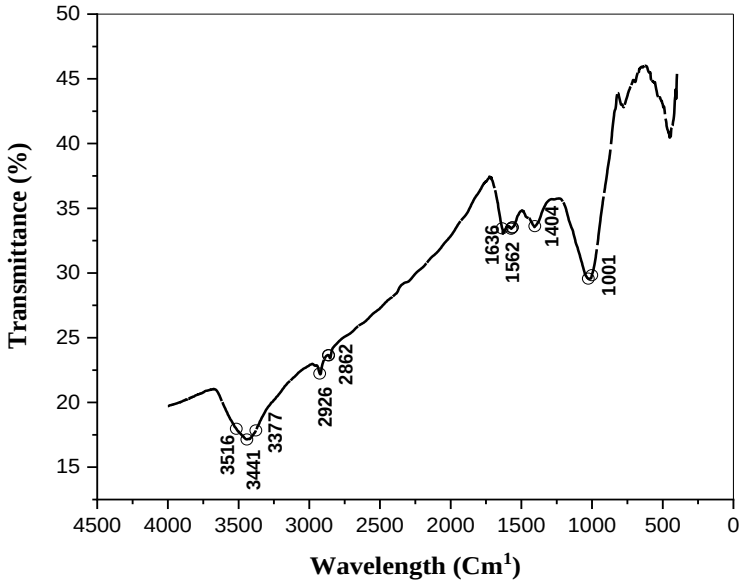

Fig. 1: FTIR spectrum of VAC

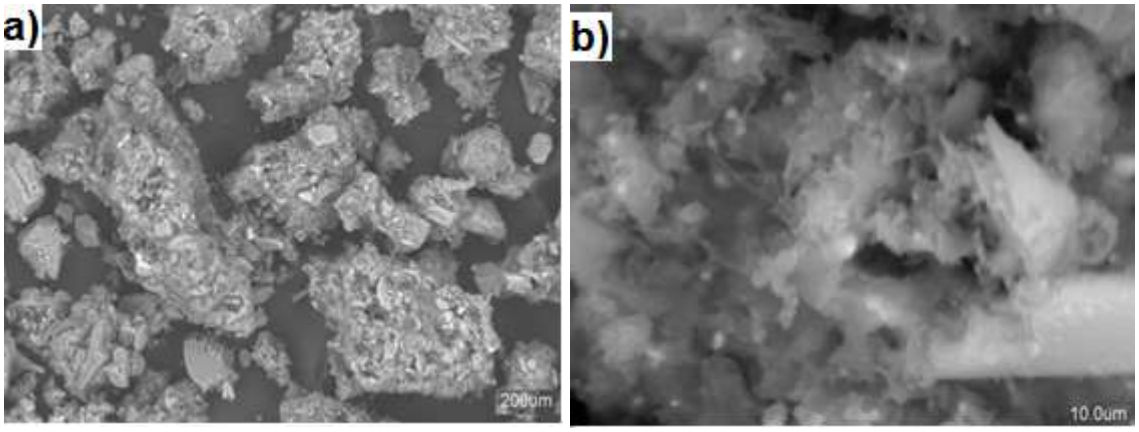

Fig. 2: SEM images of VAC at a) 200µm b) 10 µm

Table 1

Breakthrough curve parameters for single metal-ion solutions using the fixed-bed column on VAC

Metal	Feed Conc (mg L^{-1})	q_{bed} (mg g^{-1})	r_f	t_b (min)^i	t_s (min)^j	$t_{50\%}$ (min)^k
Pb^{+2}	20	0.38	530.5978	3.18	6.97	5
Cd^{+2}	20	0.53	631.4114	3.18	7.85	5.95
Ni^{+2}	20	0.59	769.3668	4	8.86	7.25

Table 2

Breakthrough curve parameters for binary metal-ion solutions using the fixed-bed column on VAC

Mixture	Feed Conc (mg L^{-1})		q_{bed} (mg g^{-1})		r_f		t_b (min)^i		t_s (min)^j		$t_{50\%}$ (min)^k	
	Metal1	Metal2	Metal1	Metal2	Metal1	Metal2	Metal1	Metal2	Metal1	Metal2	Metal1	Metal2
Pb^{+2}-Cd^{+2}	20	20	0.36	0.55	769.37	848.96	2.53	2.51	7.25	8	4.5	5.35
Pb^{+2}-Ni^{+2}	20	20	0.32	0.25	822.43	716.31	3.21	2.55	7.75	6.75	5.5	4.75
Cd^{+2}-Ni^{+2}	20	20	0.24	0.43	727.98	843.65	2.88	3.51	6.86	7.95	5	5.85

$^i t_b$ at C_t/C_o=0.2, Metal1, Metal2 being the first and second metal in a mixture.
$^j t_s$ C_t/C_o=0.8; $^k t_{50\%}$ C_t/C_o=0.5

Breakthrough parameters were plotted for experimental versus ANNs models based on four surrogate models (FFBP, FFBP-DTD, Cascade and Elman) using the Levenberg-Marquardt algorithm in single and binary feed solutions as shown in fig. 4. The breakthrough analysis was performed using one or two hidden layers, having 8 to 10 neurons inside every layer. For all the metal ions in single and binary solutions, FFBP model fitted very well in all the conditions. FFBP-DTD represented a deviation from the fit, Cascade network fitted well for Pb^{+2} in single as well as for binary (Pb^{+2} - Cd^{+2}) system and Elman network fitted well for Ni^{+2} in single and Pb^{+2} in binary (Pb^{+2}- Ni^{+2}) systems respectively.

Performance Evaluation of ANNs models based on RMSE: On the basis of Root mean square error (RMSE), a comparative study on the evaluation of the ANNs models was performed. The errors were calculated for each of the models for RMSE and the equation for computation is as follows:

$$RMSE = \sqrt{\frac{\sum_{i=1}^{N}\left(Y_{pre} - Y_{\exp}\right)^2}{N-1}}$$

where N is the total number of model outputs, *Ypre* is the predicted output, and *Yexp* is the experimental value.

From table 3, it can be interpreted that the least RMSE value was achieved for FFBP model and FFBP-DTD model has the highest error for single as well as for binary feed solutions, respectively.

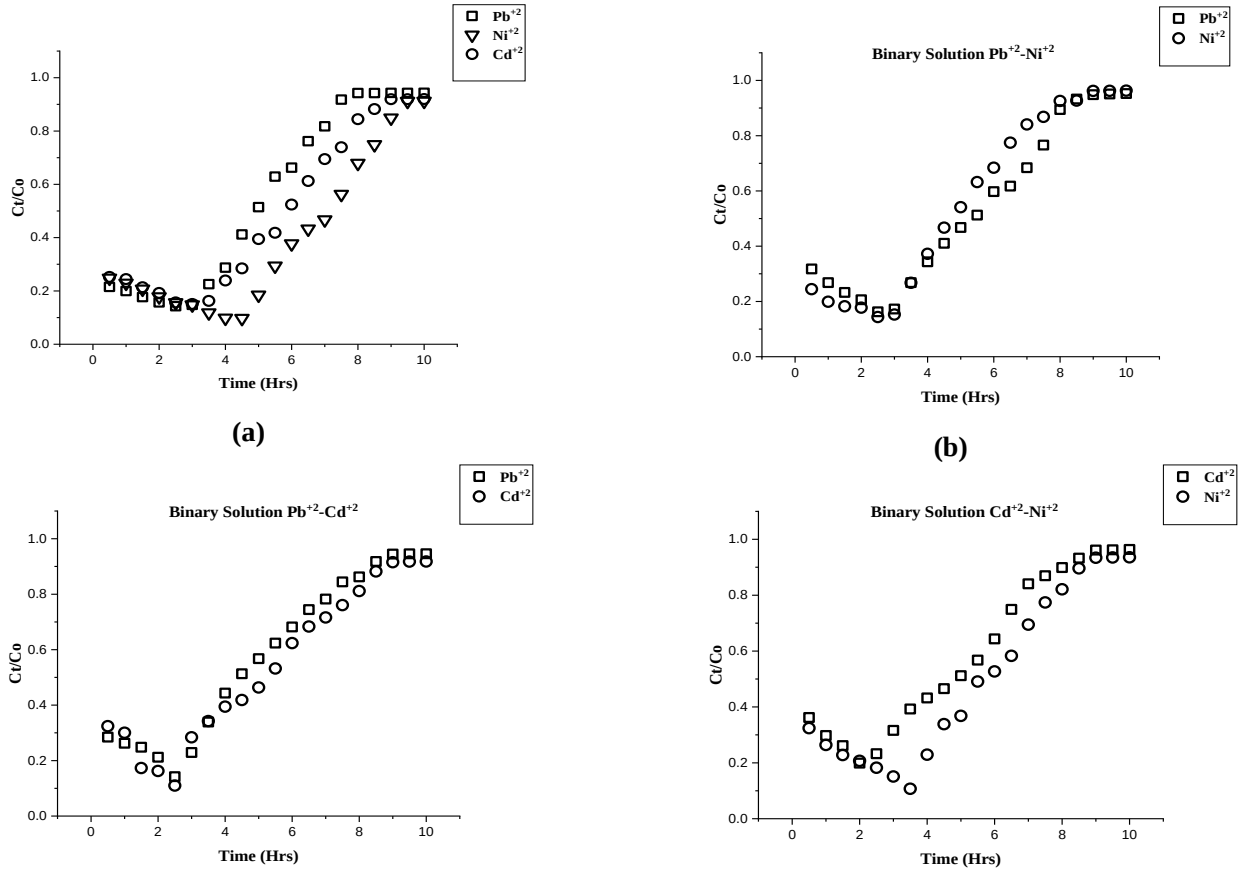

Fig. 3: Experimental Breakthrough curves for a) single metal ions b), c), d) Binary solutions

Table 3
RMSE for ANNs models for Single and Binary feed

ANNs	RMSE								
	Pb^{+2}	Cd^{+2}	Ni^{+2}	Pb^{+2}-Ni^{+2}		Pb^{+2}-Cd^{+2}		Cd^{+2}-Ni^{+2}	
				Metal 1	Metal 2	Metal 1	Metal 2	Metal 1	Metal 2
FFBP	0.000014	0.000012	0.000021	0.00003	0.000041	0.000021	0.000014	0.000015	0.000013
Cascade	0.000021	0.000035	0.000035	0.00011	0.00084	0.00032	0.00047	0.00024	0.00035
FFBP-DTD	0.00021	0.00021	0.00024	0.0023	0.0034	0.0051	0.0068	0.0031	0.0041
Elman	0.000031	0.000061	0.000045	0.00012	0.00094	0.00023	0.00087	0.00056	0.00064

Metal1, Metal2 being the first and second metal in a mixture

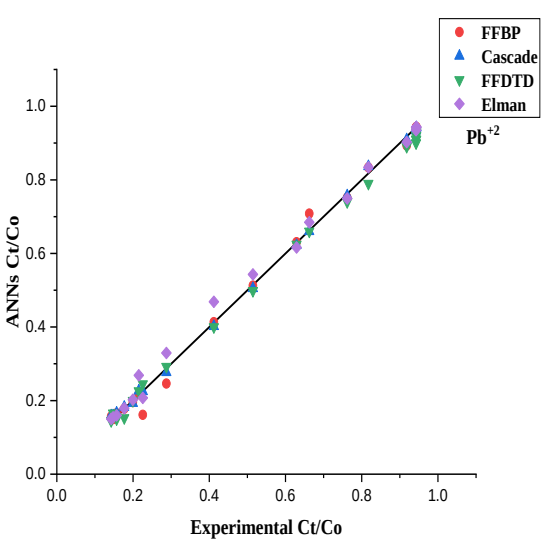
FFBP
Cascade
FFDTD
Elman
Pb+2
ANNs Ct/Co
Experimental Ct/Co

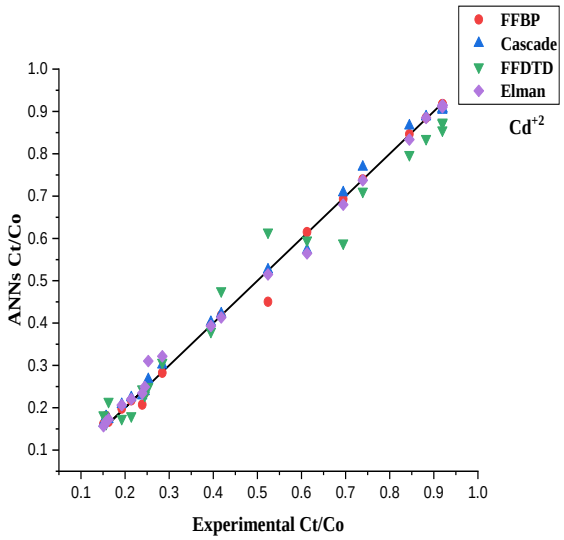
FFBP
Cascade
FFDTD
Elman
Cd+2
ANNs Ct/Co
Experimental Ct/Co

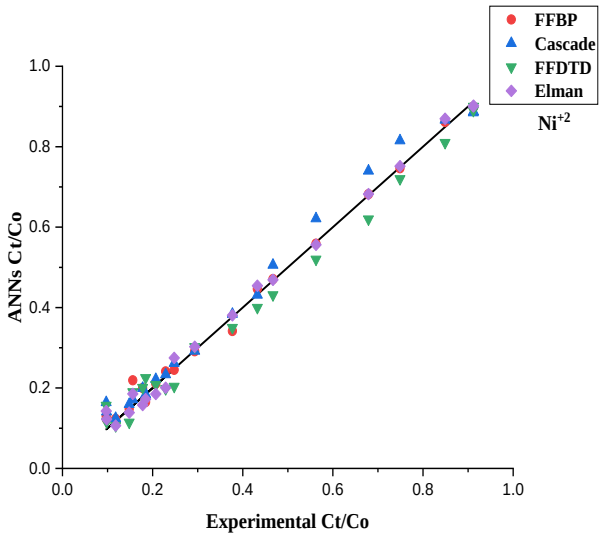
FFBP
Cascade
FFDTD
Elman
Ni+2
ANNs Ct/Co
Experimental Ct/Co

(a)

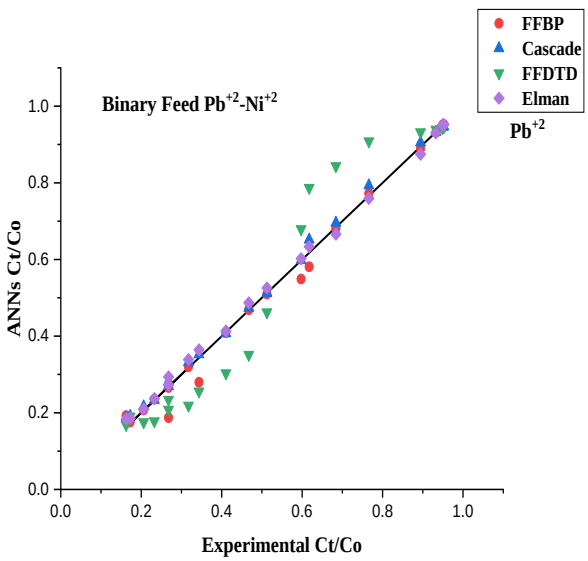
Binary Feed Pb+2-Ni+2
FFBP
Cascade
FFDTD
Elman
Pb+2
ANNs Ct/Co
Experimental Ct/Co

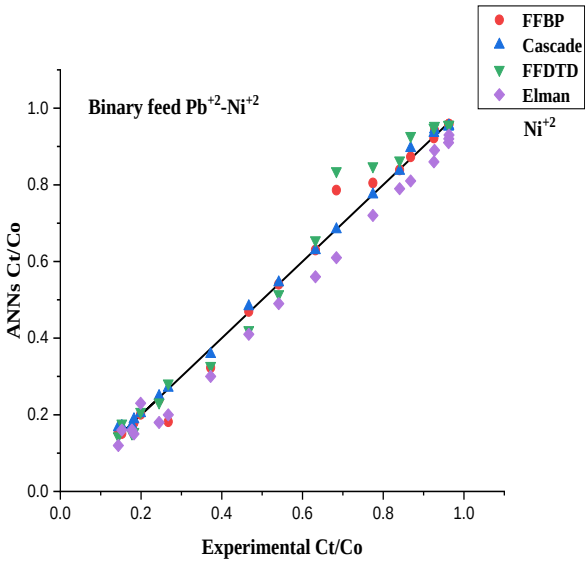
Binary feed Pb+2-Ni+2
FFBP
Cascade
FFDTD
Elman
Ni+2
ANNs Ct/Co
Experimental Ct/Co

(b)

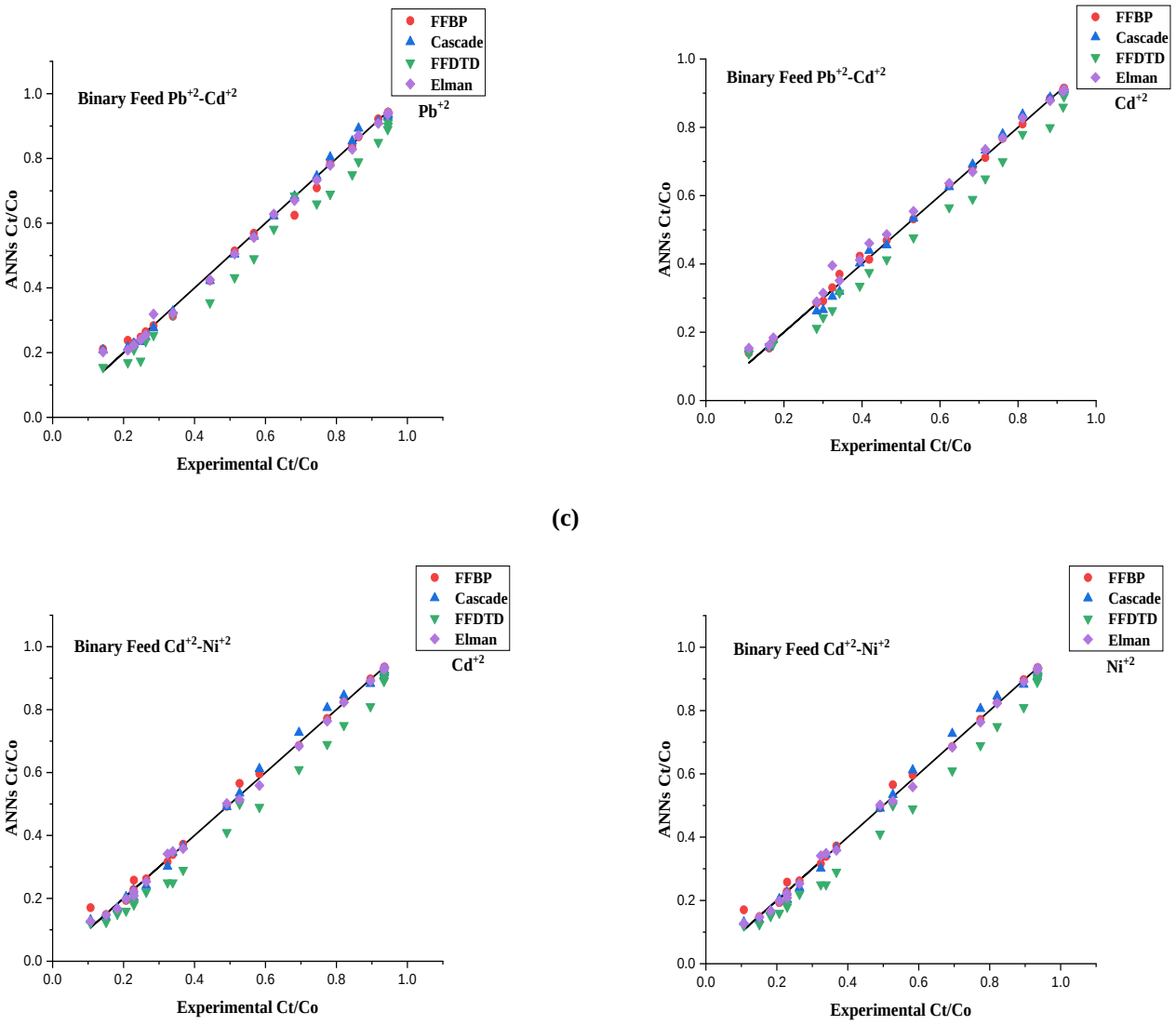

Fig. 4: Experimental versus ANNs breakthrough analysis for metal-ion adsorption onto VAC for a) single metal-ion solutions of Pb^{+2}-Ni^{+2} -$^{2}Cd^{+2}$ b)binary Feed Pb^{+2}-Ni^{+2}c) binary Feed $Pb^{+2}Cd^{+2}$ d) binary Feed Cd^{+2}-Ni^{+2}

Conclusion

The effectiveness of KOH activated *vetiver* root activated carbon (VAC) as adsorbent was investigated in removing Lead, Cadmium and Nickel from both single and multi-variant adsorption systems. VAC was characterized using FTIR for surface functional groups, and SEM analysis which indicated well-developed surface porosity. The fixed-bed column experimental results which measured highest metal-ion uptake (adsorption capacity), and the breakthrough parameters were compared to four neural network surrogate models. The numerical performance of the FFBP, FFBP-DTD, Cascade and Elman models was successfully trained, tested and validated.

The best models for breakthrough analysis were FFBP and Cascade with a minor shortcoming being the failure to reproduce the point of breakthrough. Remarkably, overall the highest performance was shown by Ni^{+2} in single and Cd^{+2} in multi-variant adsorption. Hence, it is noteworthy that the major factor influencing the sorption systems success rate depends on the co-adsorbates.

References

1. Abujazar Mohammedshadi S., Suja Fatihah, Ibrahim Anwar Ibrahim, Kabeel A.E. and Suraya Sharil, Productivity modelling of a developed inclined stepped solar still system based on actual performance and using a cascaded forward neural network model, *Journal of Cleaner Production*, **170**, 147-159 **(2018)**

2. Ansari H.R., Zarei M.J., Sabbaghi S. and Keshavarz P., A new comprehensive model for relative viscosity of various nanofluids using feedforward backpropagation MLP neural networks, *International Communications in Heat and Mass Transfer*, **91**, 1-164 **(2018)**

3. Bhosekar Atharv and Marianthi Ierapetritou, Advances in surrogate-based modelling, feasibility analysis, and optimization: A review, *Computers & Chemical Engineering*, **108**, 250-267 **(2018)**

4. Cavas Levent, Zeynelabidin Karabay, Hakan Alyuruk, Hatice Doğan and Demir Güleser K., Thomas and artificial neural network models for the fixed-bed adsorption of methylene blue by a beach waste Posidonia oceanica (L.) dead leaves, *Chemical Engineering Journal*, **171(2)**, 557-562 **(2011)**

5. de Araújo Padilha, Carlos Eduardo, Carlos Alberto de Araujo Padilha, Domingos Fabiano de Santana Souza, Jackson Araújo de Oliveira, Gorete Ribeiro de Macedo and Everaldo Silvino dos Santos, Prediction of rhamnolipid breakthrough curves on activated carbon and Amberlite XAD-2 using Artificial Neural Network and Group Method Data Handling models, *Journal of Molecular Liquids*, **206**, 293-299 **(2015)**

6. Godfrey E., Screening level study of pharmaceuticals in septic tanks, groundwater and surface water in Missoula, Montana **(2004)**

7. Ghaedi Abdol Mohammad and Azam Vafaei, Applications of artificial neural networks for adsorption removal of dyes from aqueous solution: a review, *Advances in Colloid and Interface Science*, **245**, 20-39 **(2017)**

8. Ghaedi M., Hajati S., Zare M. and Shajaripour Jaberi S.Y., Experimental design for the simultaneous analysis of malachite green and methylene blue; derivative spectrophotometry and principal component-artificial neural network, *RSC Advances*, **5(49)**, 38939-38947 **(2015)**

9. Gopinath, Akhil, Bharathi Ganesan Retnam, Arun Muthukkumaran and Kannan Aravamudan, Swift, versatile and a rigorous kinetic model-based artificial neural network surrogate for single and multi-component batch adsorption processes, *Journal of Molecular Liquids*, **297**, 111888 **(2020)**

10. Gordillo-Ruíz F.A., Sánchez-Ruíz F.J., Mendoza-Castillo D.I., Reynel-Ávila H.E. and Bonilla-Petriciolet A., Dynamic fuzzy neural network for simulating the fixed-bed adsorption of cadmium, nickel, and zinc on bone char, *International Journal of Environmental Science and Technology*, **15(5)**, 915-926 **(2018)**

11. Guijarro-Aldaco A., Hernandez-Montoya V., Bonilla-Petriciolet A., Montes-Moran M.A. and Mendoza-Castillo D.I., Improving the adsorption of heavy metalsfrom water using commercial carbons modified with eggshell wastes, *Ind. Eng.Chem. Res*, **50**, 9354–9362 **(2011)**

12. Hernández-Hernández L.E., Bonilla-Petriciolet A., Mendoza-Castillo D.I. and Reynel-Ávila H.E., Antagonistic binary adsorption of heavy metals using stratified bone char columns, *Journal of Molecular Liquids*, **241,** 334-346 **(2017)**

13. Acero J.L., Benitez F.J., Real F.J. and Teva F., Removal of emerging contaminants from secondary effluents by micellar-enhanced ultrafiltration, *Sep. Purif. Technol*., **181**, 123–131 **(2017)**

14. Jain M., Garg V.K., Kadirvelu K. and Sillanpää M., Adsorption of heavy metals from multi-metal aqueous solution by sunflower plant biomass-based carbons, *Int. J Environ Sci Technol*., **13**, 493–500 **(2016)**

15. Jamshidi M., Ghaedi M., Dashtian K., Ghaedi A.M., Hajati S., Goudarzi A. and Alipanahpour E., Highly efficient simultaneous ultrasonic-assisted adsorption of brilliant green and eosin B onto ZnS nanoparticles loaded activated carbon: artificial neural network modelling and central composite design optimization, *Spectrochimica Acta Part A: Molecular and Biomolecular Spectroscopy*, **153**, 257-267 **(2016)**

16. Lashkarbolooki Mostafa, Zeinab Sadat Shafipour and Ali Zeinolabedini Hezave, Trainable cascade-forward backpropagation network modelling of spearmint oil extraction in a packed bed using SC-CO_2, *The Journal of Supercritical Fluids*, **73**, 108-115 **(2013)**

17. Mendoza-Castillo D.I., Reynel-Ávila H.E., Sánchez-Ruiz F.J., Trejo-Valencia R., Jaime-Leal J.E. and Bonilla-Petriciolet A., Insights and pitfalls of artificial neural network modelling of competitive multi-metallic adsorption data, *Journal of Molecular Liquids*, **251**, 15-27 **(2018)**

18. Meng Hongying, Nadia Bianchi-Berthouze, Yangdong Deng, Jinkuang Cheng and Cosmas John P., Time-delay neural network for continuous emotional dimension prediction from facial expression sequences, *IEEE Transactions on Cybernetics*, **46(4)**, 916-929 **(2015)**

19. Montgomery D.C., Design and Analysis of Experiments, John Wiley and Sons, New York **(2017)**

20. Ruiz Baca Luis G., Rueda R., Cuéllar Manuel P. and Pegalajar M.C., Energy consumption forecasting based on Elman neural networks with evolutive optimization, *Expert Systems with Applications*, **92**, 380-389 **(2018)**

21. Manjunath S.V., Kumar S.M., Ngo H.H. and Guo W., Metronidazole removal in powder activated carbon and concrete-containing graphene adsorption systems: Estimation of kinetic, equilibrium and thermodynamic parameters and optimization of adsorption by a central composite design, *J. Environ. Sci. Heal.* - Part A, **52**, 1269–1283 **(2017)**

22. Tomczak and Elwira, Application of ANN and EA for the description of metal ions sorption on chitosan foamed structure—Equilibrium and dynamics of the packed column, *Computers & Chemical Engineering*, **35(2)**, 226-235 **(2011)**

23. Gamze Turan N., Basak Mesci and Okan Ozgonenel, The use of artificial neural networks (ANN) for modelling of adsorption of Cu (II) from industrial leachate by pumice, *Chemical Engineering Journal*, **171(3),** 1091-1097 **(2011)**

24. Wang Jujie, Wenyu Zhang, Yaning Li, Jianzhou Wang and Zhangli Dang, Forecasting wind speed using empirical mode decomposition and Elman neural network, *Applied Soft Computing*, **23**, 452-459 **(2014)**

25. Worch Eckhard, Competitive adsorption of micropollutants and NOM onto activated carbon: comparison of different model approaches, *Journal of Water Supply: Research and Technology—AQUA*, **59(5)**, 285-297 **(2010)**

26. Wang Y., Han T., Xu Z., Bao G. and Zhu T., Optimization of phosphorus removal from secondary effluent using the simplex method in Tianjin, China, *J. Hazard Mater*, **121**, 183–186 **(2005)**.

(Received 22nd May 2020, accepted 27th July 2020)